Journal of Innovative Optical Health Sciences
1950023 (7 pages)

DOI: 10.1142/S1793545819500238

Super-resolution microscopy based on parallel detection

Zhimin Zhang[*,‡‡], Shaocong Liu[*,‡‡], Liang Xu[*], Yubing Han[*], Cuifang Kuang[*,†,‡,‖,††], Yong Liu[§,**,††], Xiang Hao[*], Hongqin Yang[*,¶] and Xu Liu[*,‡]

[*]*State Key Laboratory of Modern Optical Instrumentation*
College of Optical Science and Engineering, Zhejiang University
Hangzhou, Zhejiang 310027, P. R. China

[†]*Ningbo Research Institute, Zhejiang University*
Ningbo 315100, P. R. China

[‡]*Collaborative Innovation Center of Extreme Optics, Shanxi University*
Taiyuan, Shanxi 030006, P. R. China

[§]*College of Electronics and Information Engineering*
Shanghai University of Electric Power, Shanghai 200090, P. R. China

[¶]*Key Laboratory of Optoelectronic Science and*
Technology for Medicine Ministry of Education and
Fujian Provincial Key Laboratory for Photonics Technology
Fujian Normal University, Fuzhou 350007, P. R. China
[‖]*cfkuang@zju.edu.cn*
[**]*liuyong7612@sina.com*

Received 11 January 2019
Accepted 28 June 2019
Published 2 October 2019

Image scanning microscopy based on pixel reassignment can improve the confocal resolution limit without losing the image signal-to-noise ratio (SNR) greatly [C. J. R. Sheppard, "Super-resolution in confocal imaging," *Optik* **80**(2) 53–54 (1988). C. B. Müller, E. Jörg, "Image scanning microscopy, "*Phys. Rev. Lett.* **104**(19) 198101 (2010). C. J. R. Sheppard, S. B. Mehta, R. Heintzmann, "Superresolution by image scanning microscopy using pixel reassignment," *Opt. Lett.* **38**(15) 2889–2892 (2013)]. Here, we use a tailor-made optical fiber and 19 avalanche photodiodes (APDs) as parallel detectors to upgrade our existing confocal microscopy, termed as parallel-detection super-resolution (PDSR) microscopy. In order to obtain the correct shift value, we use the normalized 2D cross correlation to calculate the shifting value of each image. We characterized our system performance by imaging fluorescence beads and applied this system to observing the 3D structure of biological specimen.

Keywords: Pixel reassignment; SIM; parallel-detection super-resolution (PDSR) microscopy; normalized cross-correlation algorithm.

††Corresponding authors.
‡‡Zhimin Zhang and Shaocong Liu are contributed equally to this work.

1. Introduction

Since the Abbe's diffraction limit theory[4,5] was proposed, it is well known that the conventional microscope can not achieve higher resolution surpassing the diffraction limit. The image for fine construction will be blurred by the point spread function (PSF) of the optical system. Fluorescence microscopy is a very successful technique for imaging the vital activity inside biological samples labeled with specific fluorescent probes. The best classical fluorescence microscopy can achieve lateral resolution to ca. 200 nm and axial resolution to ca. 500 nm. However, using special methods based on fluorescence, Steven Hell, Moerner and Eric Betzig, the Nobel Prize laureates in Chemistry, become well known for their contribution to the "development of super-resolution microscopy".[6–10] Up to now, numerous extraordinary methods to surpass the resolution limit have been proposed, which greatly promote the development of cytobiology.

Confocal fluorescent microscopy is one of the useful methods to improve the resolution and decrease the background noise because of the existence of pinhole. It is found that the PSF of confocal system in incoherent case would be sharpened with decreasing the size of pinhole and up to a factor of 1.4 ultimately with infinitely small pinhole.[11,12] However, the quality of image will be deteriorated because the smaller pinhole prevents more effective information out of the detector. It is obviously not practical because of the awful signal-to-noise ratio (SNR). To overcome the compromise between the resolution and SNR, the image scanning microscopy based on pixel reassignment has been promoted, which demonstrated that confocal microscopy can also achieve super-resolution by measuring the signal at each point of the detector for each scan position.[1–3] In order to measure the signal, the detector arrays can be various, such as CCD, photomultiplier tubes arrays, single-photon avalanche diode arrays.[13] In fact, the image scanning microscopy based on pixel reassignment can also be termed as spot-scanning SIM in the broadest sense of SIM as all the corresponding imaging method could be called as "SIM" as long as the sample is illuminated by an illumination pattern with specific structure.[2,14] Using the theory of SIM, it is better to understand the frequency extension process of pixel reassignment.

Here, we use a tailor-made fiber bundle and 19 available photodiodes (APDs) being parallel detectors to upgrade our confocal microscopy, termed as parallel-detection super-resolution (PDSR) microscopy. In this paper, for the sake of confirming the displacement of each detector, we calculate the normalized 2D correlation value of each images relative to the center one. We make use of the fluorescence beads to investigate the performance of our system and apply this system, furthermore, to the biological specimen and get the super-resolution 3D image.

2. Experimental Setup

Figure 1 shows a schematic of our experimental setup. We design the whole confocal module including the detector module and the XY deflecting module that are compatible to almost all confocal system. We integrate our confocal module into a Nikon TI-E inverted fluorescence microscope. The laser with wavelength of 488 nm is made by a Chinese company, SFOLT Co. Ltd in Shanghai. The XY deflecting module is a self-made 4-f galvanometers (8310K, Cambridge technology) scanning system. The objective is a Nikon 100× oil-immersion objective. The whole magnification of

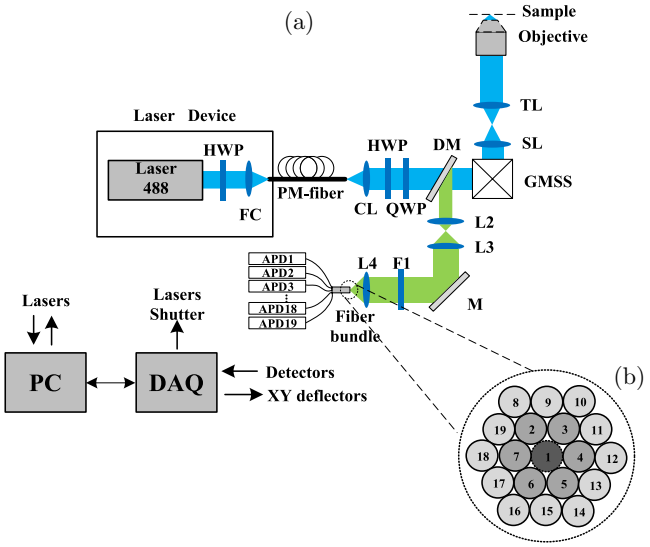

Fig. 1. Schematic of the experiment setup (a) and the fiber end of the tailor-made fiber bundle (b), which is made up of 19 isolated multi-mode fibers. FC, fiber collimator; PM-fiber, polarization maintaining fiber; CL, collimator; HWP, half wave plate; QWP, quarter wave plate; DM; dichromatic mirror; GMSS, galva mirror scan system; M, mirror; SL: scan lens, TL: tube lens, F: filter.

the system is up to a factor of 1250 and the signal will be collected by our tailor-made multi-mode fiber bundle. The diameter of each fiber is 125 μm and one end of these fibers are bundled together into one big fiber and the other end is connected with a APD (SPCM-AQRH-14-FC-ND, Digi-KEY). The 19 multi-mode fibers acting as both pinholes and signal receivers are integrated into one fiber bundle as depicted in Fig. 1(b). The diameter of each multi-mode fiber is 125 μm. At the end, the signal received by the 19 APDs is measured by four data acquisition cards (PXIe-6612, National Instrument).

It might also be noted that the great challenge during the system alignment should be the installation process of the fiber bundle as we should ensure the fluorescent intensity is decreasing from the center fiber to the edge fiber, i.e., the fluorescent intensity collected by the center fiber is the highest and the intensity from the second circle fibers is higher than the edge but lower than the center. Therefore, the Airy disk can be confirmed to be aligned with the detector array, which is significant to the reconstruction at the end.

3. Theory

3.1. *Image information and reconstruction*

In light of better understanding the frequency extension principle of pixel reassignment based on parallel detection, we will, at first, review the principle of wide-field SIM. A simplified wide-field SIM system normally uses a sinusoidal light pattern excitation.[15,16] Assuming that the magnification of the system is one, the size of image plane is corresponding with the field of sample. The pattern can be mathematically expressed as

$$h_{\text{ex}}(x) = 1 + \cos(2\pi k_e x), \tag{1}$$

where k_e is the spatial frequency of the pattern. Thus, the final image $i(x)$ can be written as

$$i(x) + (t(x) \times h_{\text{ex}}(x)) \otimes h_{\text{ob}}(x), \tag{2}$$

where $t(x)$ is the spatial density of fluorescent emitters, $h_{\text{ob}}(x)$ is the PSF of objective. The Fourier transform of $i(x)$ can be expressed as

$$\begin{aligned} I(K) &= [T(K) \otimes H_{\text{ex}}(K)] \times H_{\text{ob}}(K) \\ &= [T(k) + T(k - k_e) + T(k + k_e)] \times H_{\text{ob}}(k). \end{aligned} \tag{3}$$

This shows that, in SIM, the convolution with H_{ex} results in that the OTF of system can contain much more spatial frequency content of the sample which is up to the sum of excitation and cutoff frequency: $k_{\text{SIM}} = k + k_e$. With the help of the phase shift and rotation operation of the sinusoidal excitation pattern, it is easy to resolve the higher frequency content from different orientation of the sample and at last obtain the super-resolution image after reconstruction. It is important to note that this principle holds for any structured illumination pattern including the spot illumination in confocal microscopy.

In fact, it is easier to get the consensus that the diffraction-limited laser focus spot is a special type of structure illumination carrying all possible Fourier modes allowed by the NA of an objective.[2,14] At first, assuming that there is one detector fixed in the center optical axis, the image $I(x)$ can be derived as[14]

$$I(x) = t(x) \otimes \{h_{\text{ex}}(x) \times [h_{\text{em}}(x) \otimes d(x)]\}, \tag{4}$$

where h_{ex} and h_{em} represent the function of diffraction-limit spot in formed of the excitation and the emission through the objective, respectively. $d(x)$ is the spatial dimension of the detector. If there is only one single fluorescent emitter in the sample plane, i.e., $t(x) = \delta(x)$, $I(x)$, in other words, is the effective PSF h_{eff} of the system.

Assuming that the detector is infinitely large, we will have $d(x) = 1$ and the effective PSF h_{eff} is then equal to h_{ex}, which is equal to the PSF of wide-field microscopy without considering Stokes shift. Through Fourier transform, the effective OTF can be derived as

$$H_{\text{eff}}(k) = H_{\text{ex}}(k). \tag{5}$$

With decreasing the area of the detector, the effective PSF would be sharpened and when the detector is infinitely small, the effective PSF can be derived as

$$h_{\text{eff}}(x) = h_{\text{ex}}(x) \times h_{\text{em}}(x). \tag{6}$$

Therefore, the resolution of confocal microscopy would be enhanced with small pinhole compared with wide-field microscopy.

Assuming that the single detector is replaced with the parallel detectors, the image $I_n(x)$ depends on both the position d_n of the detector in the image plane and the scan position x in the sample

plane,[1–3,14] which can be derived as

$$I_n(x) = t(x) \otimes \{h_{\text{ex}}(x) \times [h_{\text{em}}(x) \otimes d(x + d_n)]\}, \tag{7}$$

where $d(x + d_n)$ is the spatial dimension of the detector with the position d_n. The effective PSF can also be written as

$$h_{\text{eff}}(x) = h_{\text{ex}}(x) \times h'_{\text{em}}(x + d_n). \tag{8}$$

It is easy to find that the peak value of h_{eff} will be located in the position $d_n/2$, which means that the image capture by the detector in the position x_d will result in the $d_n/2$ displacement corresponding to the center place. Thus, the effective image can be reconstructed by summing the images after translating a distance $d_n/2$ towards the center place. The effective image after reconstruction is

$$\begin{aligned} I_{\text{FS}}(x) &= \int \left[I_n(x) \otimes \delta\left(x - \frac{d_n}{2}\right) \right] dd_n \\ &= \iint t(s) h_{\text{ex}}\left(x - \frac{d_n}{2} - s\right) h_{\text{em}}\left(x + \frac{d_n}{2} - s\right) ds dd_n. \end{aligned} \tag{9}$$

It can see that the integral item of Eq. (9) is similar to Eq. (2), but the illumination pattern is replaced with a diffraction limited spot. The diffraction-limited spot h_{ex} contains all spatial frequency up to the cutoff frequency of condenser. Thus, it is possible, in principle, to extend the frequency up to double cutoff frequency of the conventional microscopy.

Substituting $u = x$, $2v = x + \frac{d_n}{2}$, the effective PSF can be rewritten as

$$h_{\text{FS}}(u) = 4 \int h_{\text{ex}}(2u - 2v) h'_{\text{em}}(2v) dv. \tag{10}$$

With Fourier transformation, the effective OTF can be derived as

$$H_{\text{FS}}(k) = 2 H_{\text{ex}}(k/2) H'_{\text{em}}(k/2), \tag{11}$$

where H_{ex} and H_{em} represent the OTF of h_{ex} and h_{em} in the frequency domain, respectively. Therefore the effective OTF after reconstruction is extended roughly up to twice comparing to a conventional wide-field microscopy, which can be seen as a frequency-extension process. However, different from wide-field SIM which only possess frequency extension in some direction, the frequency extension of PDSR takes place on every side.

3.2. *Normalized 2D correlation*

As Sec. 3.1 illustrated, it is necessary to know the displacement values of detectors. Theoretically, the fiber should be fixed exactly in the center optical axis for the best performance, as shown in Fig. 2(a), which is hard to realize in practice because of misalignment and rotational symmetry of the fiber, as shown in Fig. 2(b). To find out the influence of the back translation, we compare the effective PSF of confocal microscopy, practical PDSR microscopy with correct and wrong back translation in simulation. The fiber is transversely displaced and clockwise rotated 120° relatively to the ideal situation. The correctly reconstructed PSF with practical shifting value (see Fig. 2(d)) is apparently more sharp than the PSF of confocal microscopy as shown but the wrong reconstructed PSF (see Fig. 2(e)) with ideal shifting value is much larger than the PSF of confocal microscopy. Thus, before reconstruction, it is significant to know the exact offset of each pinhole.

As we know from Eq. (8), the displacement of detector will result in the offset of the image relatively to the center one. Therefore, the reconstruction can be obtained easily if we can calculate the offset of the images. Here, we utilize a fast normalized cross-correlation algorithm[17] to calculate the offset of each image by calculating the correlation coefficient of each image relative to the image captured from the center detector, which could

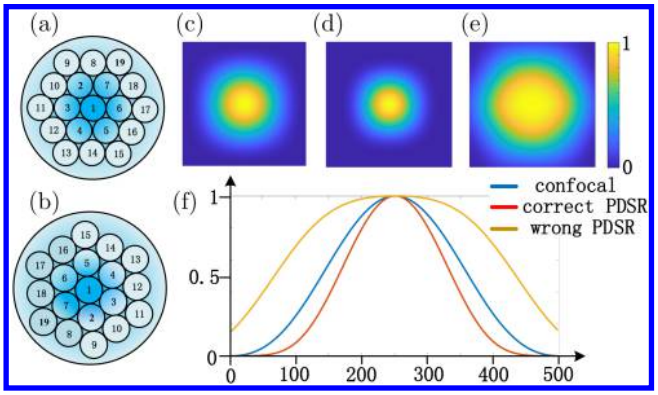

Fig. 2. Illustration of the reconstruction with correct shifting value and wrong shifting value. The ideal condition (a) and the practical condition (b) of the fiber in the setup. The PSF of confocal (c), correct reconstruction (d) and wrong reconstruction (e). The normalized intensity profile of cross-section through the PSF of confocal, correct reconstruction and wrong reconstruction (f). The color bar represents the normalized intensity.

be derived as

$$c_n(u,v) = \frac{\sum_{x,y}[I_n(x,y)-\bar{I}_{n(u,v)}][I_1(x-u,y-v)-\bar{I}_1]}{\left\{\sum_{x,y}\left[I_n(x,y)-\bar{I}_{n(u,v)}\right]^2 \sum_{x,y}\left[I_1(x-u,y-v)-\bar{I}_1\right]^2\right\}^{0.5}} \quad n = 2,3,\ldots,19, \tag{12}$$

where I_n is the image captured by the Nth detector and the $\bar{I}_{n(u,\nu)}$ is the mean of I_n in the region under the feature. I_1 is the center image and $\bar{I}_1$ is the mean of I_1. The coordinates of the max coefficient should be found out after the calculation of Eq. (12), then the exact displacement of each image can be obtained with the coordinate and the given displacement.

4. Results and Discussion

4.1. *Imaging fluorescent beads*

We characterized our system performance by imaging fluorescence beads with size of 100 nm. Sample scanning was performed with 6 μs acquisition time per scan position and scan step size of 20 nm. And the detector module is composed with 19 APDs as parallel detectors.

The fluorescence beads were excited by the wavelength of 488 nm. We measured the full width at half maximum (FWHM) of a single fluorescence bead to characterize the resolution of PDSR microscope. Compared with the conventional confocal microscopy, PDSR can achieve the lateral resolution up to 120 nm ± 20 nm at a single 100 nm diameter fluorescence bead, as shown in Fig. 3(c). Furthermore, we also compare the profile of some overlapped fluorescence beads, which are placed at the distance below the diffraction limit. The profile line (see Fig. 3(d)) shows us that the three fluorescence beads, which are placed in the straight line region with length of 400 nm, can be distinguished in PDSR but hard in the conventional confocal microscopy.

4.2. *Imaging biological samples*

To investigate the performance of our system for the biological imaging, including 2D and 3D images, we imaged the microtubules in human osteosarcoma (U20S) cell labeled with Alexa plus 488. We compared the performance between the conventional confocal microscopy and PDSR microscopy.

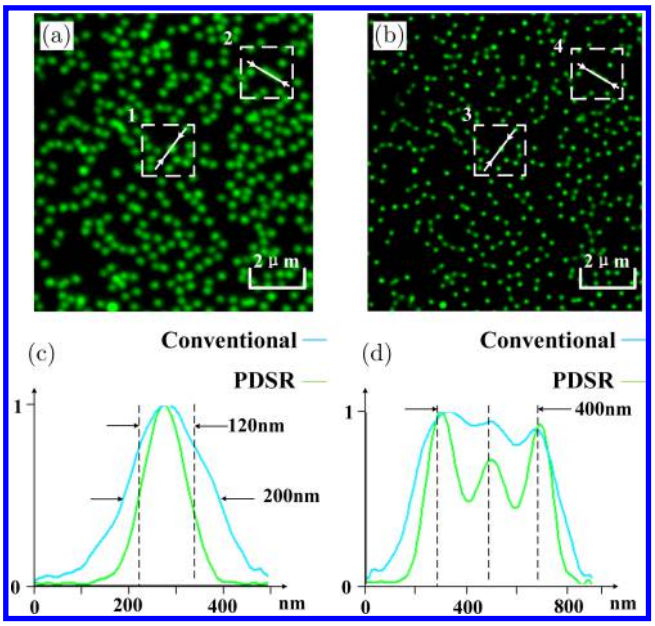

Fig. 3. Resolution enhancement realized by PDSR microscopy. The diameter of fluorescence bead is 100 nm. (a) The image captured by conventional confocal laser scanning microscopy. (b) The image captured by PDSR microscopy. (c) The normalized line profiles of the single fluorescence bead along the traces indicated by white line in the Nos. 1 and Nos. 3 dashed box region. (d) The normalized line profiles of fluorescence beads along the traces indicated by white line in the Nos. 2 and Nos. 4 dashed box region. Scale bar: 2 μm.

As shown in Fig. 4, the field of view is 15 μm × 15 μm with 6 μs acquisition time per pixel and 30 nm step size.

As shown in Figs. 4(a) and 4(b), it is easy to find that PDSR can greatly improve the resolution and contrast comparing the conventional confocal microscopy. Depicting a normalized line profile along the trace indicated by the white line, we can find that in PDSR microscopy, two peaks of microtubules, away from 240 nm, can still be determined but hardly distinguished in the conventional confocal microscopy.

Furthermore, we also explored the 3D performance of PDSR microscopy compared to the conventional confocal microscopy. As shown in Fig. 5, for a 4.7 μm thick volume, we acquired 94 slices spaced 50 nm apart at a 2D imaging rate of 6 μs per scan position.

A cross-section (see Fig. 5(f), captured from the conventional confocal microscopy and Fig. 5(e), captured from the PDSR microscopy) along the oblique line depicted in Fig. 5(c)) is used to characterize the axial resolution performance of PDSR microscopy. The result shows that PDSR cannot

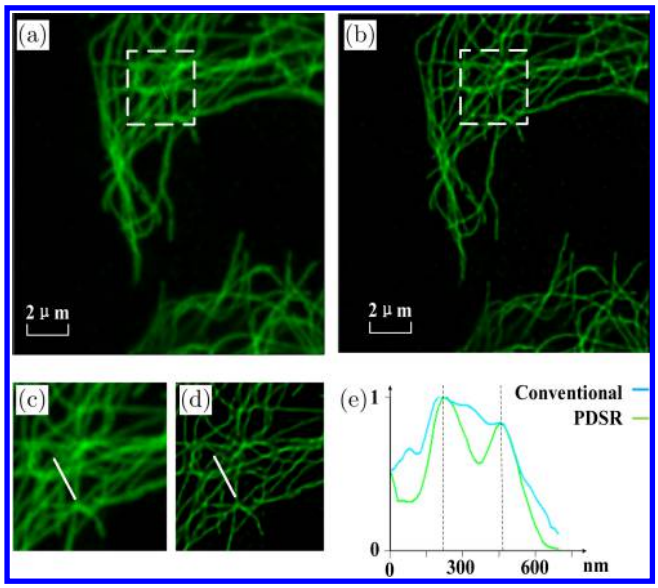

Fig. 4. The images of a fixed U20S cell captured by conventional confocal microscopy and PDSR microscopy. (a) The image captured by conventional microscopy. (b) The image captured by PDSR microscopy. (c, d) The local area indicated, respectively, in the dashed box in (a) and (b). (e) The line profiles along the traces indicated by white line. The images were captured with 6 μs acquisition time per pixel and 30 nm step size per scan position. The microtubules were labeled by Alexa plus 488. Scale bar: 2 μm.

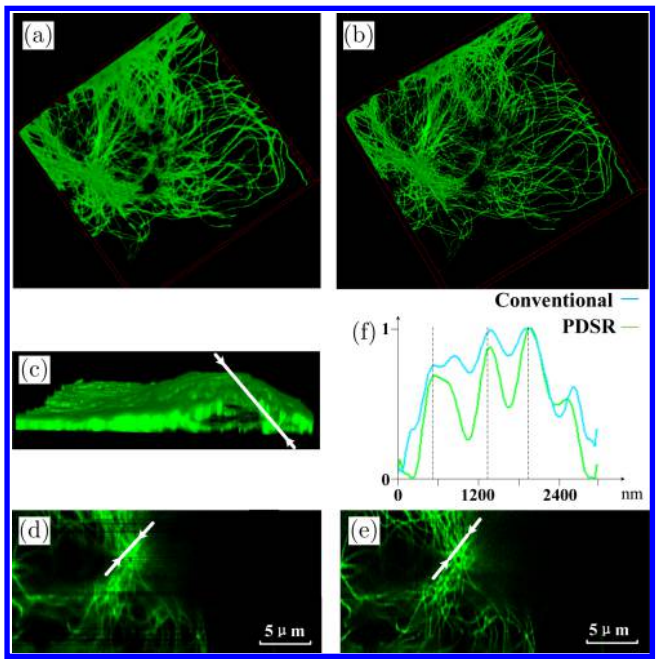

Fig. 5. The 3D image of a fixed U2OS cell captured by conventional confocal microscopy and PDSR microscopy. The top view of conventional confocal microscopy (a) and PDSR microscopy (b). The front side image (c) of (a). The oblique images (d, e) along the direction of white line indicated in c is, respectively, extracted from (a) and (b). The line profiles (f) along the trace indicated by the white line in (d) and (e). Scale bar: 5 μm.

only enhance the lateral resolution but also the axial resolution comparing the conventional confocal microscopy. We drew a normalized line profile (see Fig. 5(f)) along the white line depicted in Figs. 5(d) and 5(e). Three peaks along the axial direction can be easily distinguished in PDSR but slightly harder in the conventional confocal microscopy.

5. Conclusion

SIM is a useful technique suitable for live cell research because of its' flexible operation and broad application for various fluorescent dyes.[18,19] Image scanning microscopy using a focused spot as structured illumination pattern to extend the application of SIM to the confocal microscopy. Our PDSR microscopy system is much more flexible than other system because we just use a tailor-made fiber and 19 detectors to upgrade our existing fluorescence confocal to a super-resolution microscopy without any other cost. In contrast to the conventional confocal microscopy, our PDSR system can surpassing the lateral resolution limit by a factor of 1.6 and also slightly improve the axial resolution. It is worth noting that parallel detector module can be not only integrated to confocal microscopy but also applicable for other spot scanning microscopy, e.g., STED microscopy and fluorescence emission difference (FED) microscopy.[20] Recently, there are many methods using doughnut-spot excitation and the parallel detection to further enhance the resolution.[21–23]

However, in other words, there are some critical problem existing in our system. First of all, scanning speed restricts potential of PDSR to explore the higher dynamic process of live cell. One possible solution is to use the parallel excitation to improve the imaging speed, like MSIM, proposed by York, which uses DMD to form a 2D spot pattern to accelerate the scanning speed.[24] In addition, the axial resolution of PDSR is still limit. Modulation of the axial illumination pattern would be potential solution to improve the axial resolution, just like 3D SIM.[25,26] Another way we can achieve is to apply 3D doughnut spot to our system, which will be our next research work.

Acknowledgments

This work was financially sponsored by National Natural Science Foundation of China (61827825

and 61735017), Fundamental Research Funds for the Central Universities (2019XZZX003-06), Natural Science Foundation of Zhejiang province (LR16F050001), and Zhejiang Lab (2018EB0ZX01).

References

1. C. J. R. Sheppard, "Super-resolution in confocal imaging," *Optik* **80**(2), 53–54 (1988).
2. C. B. Müller, E. Jörg, "Image scanning microscopy," *Phys. Rev. Lett.* **104**(19), 198101 (2010).
3. C. J. R. Sheppard, S. B. Mehta, R. Heintzmann, "Superresolution by image scanning microscopy using pixel reassignment," *Opt. Lett.* **38**(15), 2889–2892 (2013).
4. E. Abbe, "Beiträge zur Theorie des Mikro skops und der mikroskopischen Wahrnehmung," *Archiv für mikroskopische Anatomie* **9**(1), 413–418 (1873).
5. C. Hockin, "On the estimation of aperture in the microscope," *J. R. Microscop. Soc.* **4**(3), 337–347 (1884).
6. S. W. Hell, W. Jan, "Breaking the diffraction resolution limit by stimulated emission: Stimulated-emission-depletion fluorescence microscopy," *Opt. Lett.* **19**(11), 780–782 (1994).
7. W. E. Moerner, L. Kador, "Optical detection and spectroscopy of single molecules in a solid," *Phys. Rev. Lett.* **62**(21), 2535 (1989).
8. E. Betzig, "Proposed method for molecular optical imaging," *Opt. Lett.* **20**(3) 237–239 (1995).
9. S. T. Hess, T. P. K. Girirajan, M. D. Mason, "Ultra-high resolution imaging by fluorescence photo-activation localization microscopy," *Biophys. J.* **91**(11), 4258–4272 (2006).
10. X. Wang *et al.*, "Super-resolution microscopy and its applications in neuroscience," *J. Innov. Opt. Health Sci.* **10**(5), 1730001 (2017).
11. C. J. R. Sheppard, A. Choudhury, "Image formation in the scanning microscope," *Opti. Acta. Int. J. Optics* **24**(10), 1051–1073 (1977).
12. G. Cox, C. J. R. Sheppard, "Practical limits of resolution in confocal and non-linear microscopy," *Microsc. Res. Tech.* **63**(1), 18–22 (2004).
13. M. Castello *et al.*, "A robust and versatile platform for image scanning microscopy enabling super-resolution FLIM," *Nat. Methods* **16**(2), 175 (2019).
14. F. Ströhl, C. F. Kaminski, "Frontiers in structured illumination microscopy," *Optica* **3**(6), 667–677 (2016).
15. R. Heintzmann, C. G. Cremer, "Laterally modulated excitation microscopy: Improvement of resolution by using a diffraction grating," *Opt. Biopsies Microsc. Techn. III* **3568** (1999), International Society for Optics and Photonics.
16. M. G. L. Gustafsson, "Surpassing the lateral resolution limit by a factor of two using structured illumination microscopy," *J. Microsc.* **198**(2), 82–87 (2000).
17. J.-C. Yoo, T. H. Han, "Fast normalized cross-correlation, *Circuits Syst. Signal Process.* **28**(6), 819 (2009).
18. Y. He *et al.*, "Rapid bacteria identification using structured illumination microscopy and machine learning," *J. Innov. Opt. Health Sci.* **11**(1), 1850007 (2018).
19. X. Yang *et al.*, "Fringe optimization for structured illumination super-resolution microscope with digital micromirror device," *J. Innov. Opt. Health Sci.* **12**(3), 1950014 (2019).
20. C. Kuang *et al.*, "Breaking the diffraction barrier using fluorescence emission difference microscopy," *Sci. Rep.* **3**, 1441 (2013).
21. Y. Ma *et al.*, "Virtual fluorescence emission difference microscopy based on photon reassignment," *Optics Lett.* **40**(20), 4627–4630 (2015).
22. B. Ge *et al.*, "Three-dimensional resolution and contrast-enhanced confocal microscopy with array detection," *Optics Lett.* **41**(9), 2013–2016 (2016).
23. S. Liu *et al.*, "Saturated virtual fluorescence emission difference microscopy based on detector array," *Opt. Commun.* **395**, 45–50 (2017).
24. A. G. York *et al.*, "Resolution doubling in live, multicellular organisms via multifocal structured illumination microscopy," *Nat. Methods* **9**(7), 749 (2012).
25. M. G. L. Gustafsson *et al.*, "Three-dimensional resolution doubling in wide-field fluorescence microscopy by structured illumination," *Biophys. J.* **94**(12), 4957–4970 (2008).
26. L. Schermelleh *et al.*, "Subdiffraction multicolor imaging of the nuclear periphery with 3D structured illumination microscopy," *Science* **320**(5881), 1332–1336 (2008).